`dcemri`: A Package for Medical Image Analysis

Brandon Whitcher
bjw34032@users.sourceforge.net
Volker J. Schmid
volkerschmid@users.sourceforge.net

July 10, 2009

1   Introduction

Quantitative analysis of perfusion imaging using dynamic contrast-enhanced MRI (DCE-MRI) is achieved through a series of processing steps, starting with the raw data acquired from the MRI scanner, and involves a combination of physics, mathematics, engineering and statistics. The purpose of the **dcemri** package is to provide a collection of functions that move the experimental data through all steps of the data analysis pipeline using standard data formats that may be visualized and manipulated across a wide variety of software packages.

2   Data Input/Output

The **dcemri** package requires incoming data to be in the ANALYZE 7.5 or NIfTI formats. Data conversion (e.g., from DICOM to NIfTI) must be performed by the user before **dcemri** may be used to summarize the data. Several software packages allow DICOM-to-NIfTI (or ANALYZE) conversion; e.g.,

- FreeSurfer (surfer.nmr.mgh.harvard.edu)

- Xmedcon (xmedcon.sourceforge.net)

- MRIConvert (lnci.oregon.edu/~jolinda/MRIConvert)

This is by no means an exhaustive list of software available for DICOM conversion.

2.1   Labelled LR Standard (MNI152) Images in NIfTI Format

The first example of reading in, and displaying, medical imaging data in NIfTI format (avg152T1_LR_nifti.nii.gz) was obtained from the NIfTI website (nifti.nimh.nih.gov/nifti-1/). Successful execution of the command

```
> mni <- read.img("avg152T1_LR_nifti.nii.gz")
> dim(mni)
```

```
[1]  91 109  91
```

produces a 3D array of the image data that may be displayed in a 10×10 grid of images (Figure 1).
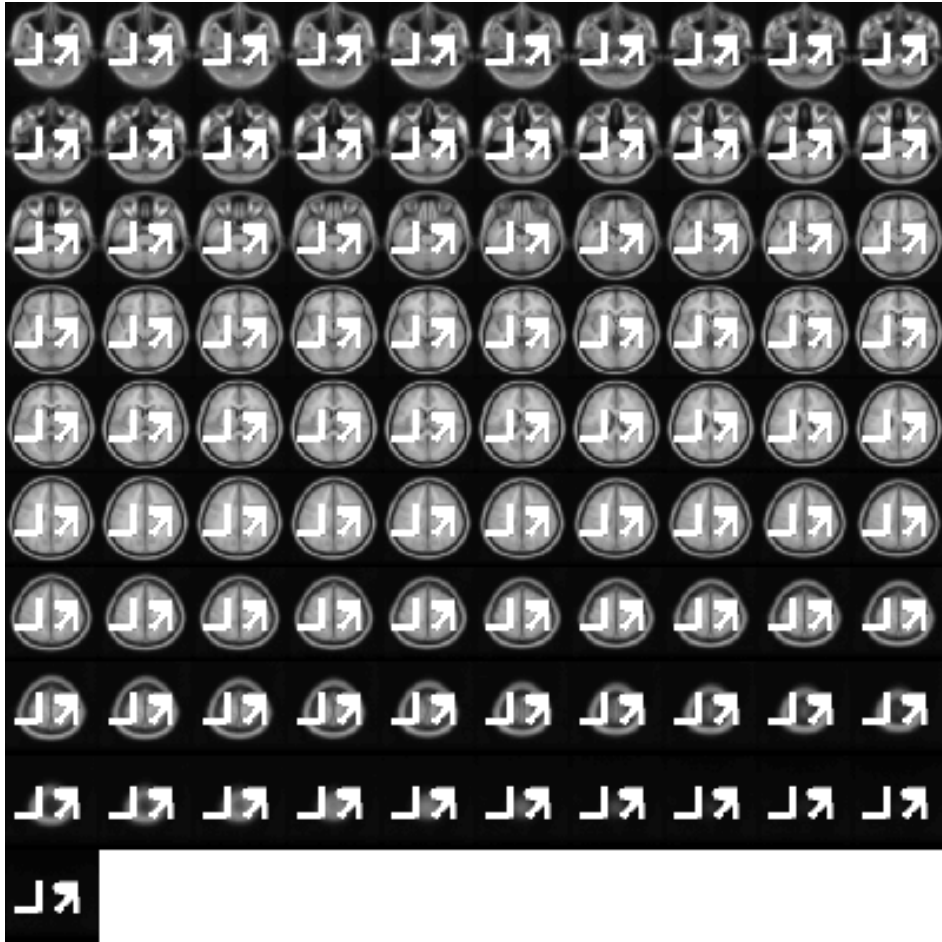

Figure 1: Axial slices of MNI volume `avg152T1_LR_nifti` stored in radiological convention.

The second example of reading in, and displaying, medical imaging data in NIfTI format (`avg152T1_RL_nifti.nii`) was also obtained from the NIfTI website (nifti.nimh.nih.gov/nifti-1/). Successful execution of the command

```
> mni <- read.img("avg152T1_RL_nifti.nii.gz")
> dim(mni)
```

```
[1]  91 109  91
```

produces a 3D array of the image data that may be displayed in a 10×10 grid of images (Figure 2).

The first image (LR) is stored in radiological convention. The second image (RL) is stored in neurological convention. Any NIfTI-1 compliant viewing software should display these images identically.
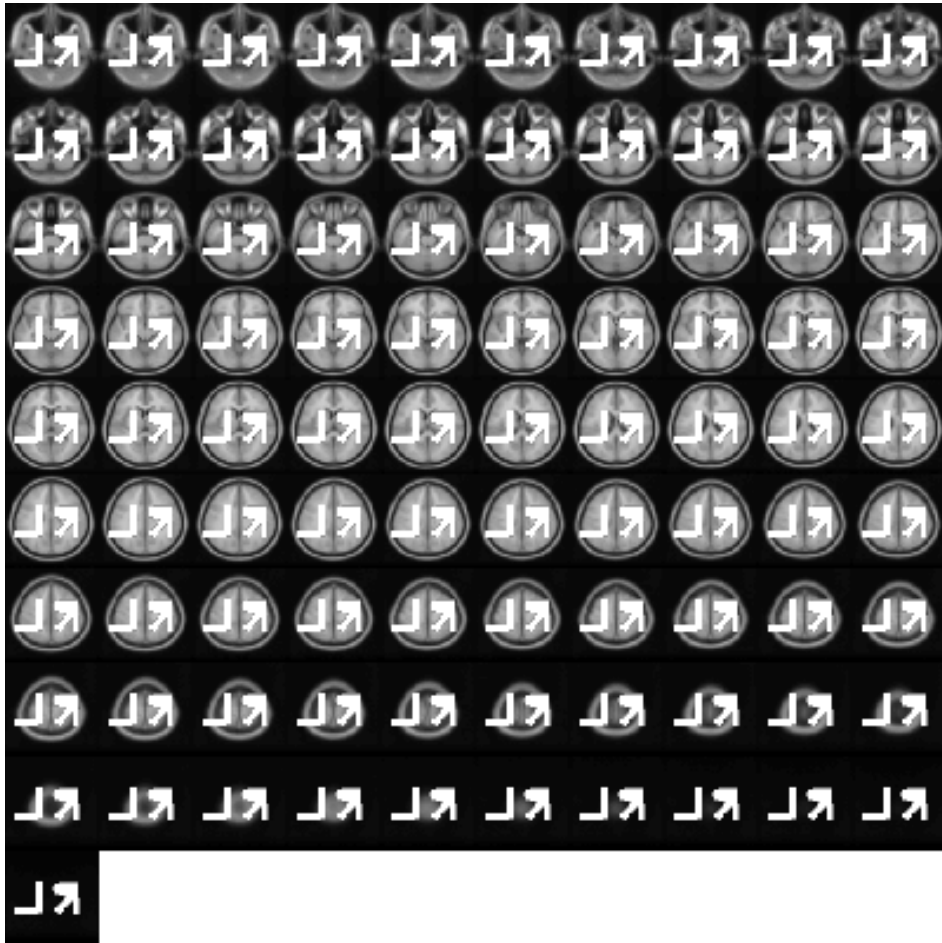
Figure 2: Axial slices of MNI volume `avg152T1_RL_nifti` stored in neurological convention.

2.2   Simple Time-series or Multi-volume Image

This is an example of reading in, and displaying, a four-dimensional medical imaging data set in NIfTI format (`filtered_func_data.nii`) obtained from the NIfTI website (nifti.nimh.nih.gov/nifti-1/). Successful execution of the command

```
> ffd <- read.img("filtered_func_data.nii.gz")
> dim(ffd)

[1]  64  64  21 180
```

produces a four-dimensional (4D) array of imaging data that may be displayed in a 5×5 grid of images (Figure 3). The first three dimensions are spatial locations of the voxel (volume element) and the fourth dimension is time.
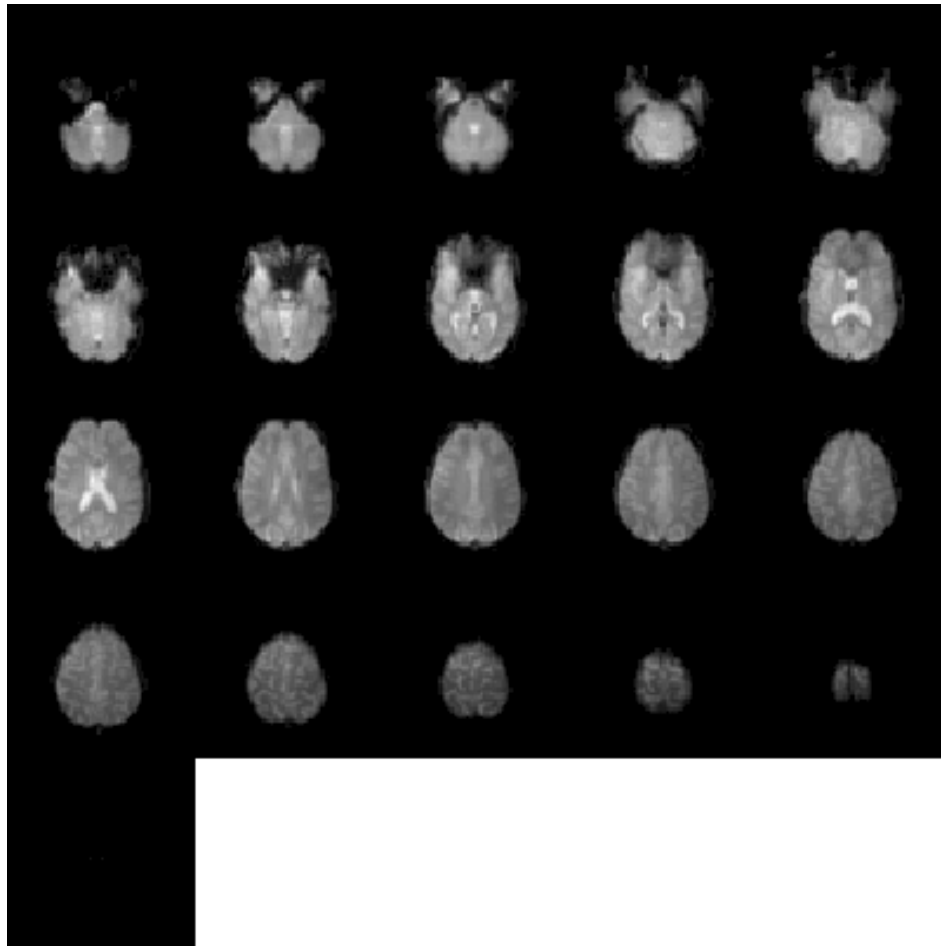

Figure 3: Axial slices of the functional MRI "volume" `filtered_func_data` from the first acquisition.

2.3 Statistic Image

This is an example of reading in and displaying a statistical image so that it may be overlayed on the EPI (echo planar imaging) data taken from the functional MRI experiment. The original NIfTI files (`filtereted_func_data.nii` and `zstat1.nii`) were obtained from the NIfTI website (nifti.nimh.nih.gov/nifti-1/). Successful execution of the command

```
> zstat1 <- read.img("zstat1.nii.gz")
> dim(zstat1)

[1] 64 64 21
```

produces a 3D array of parameter estimates (essentially coefficients from a linear regression performed at each voxel) that may be overlayed on the original data for anatomical reference (Figure 4).
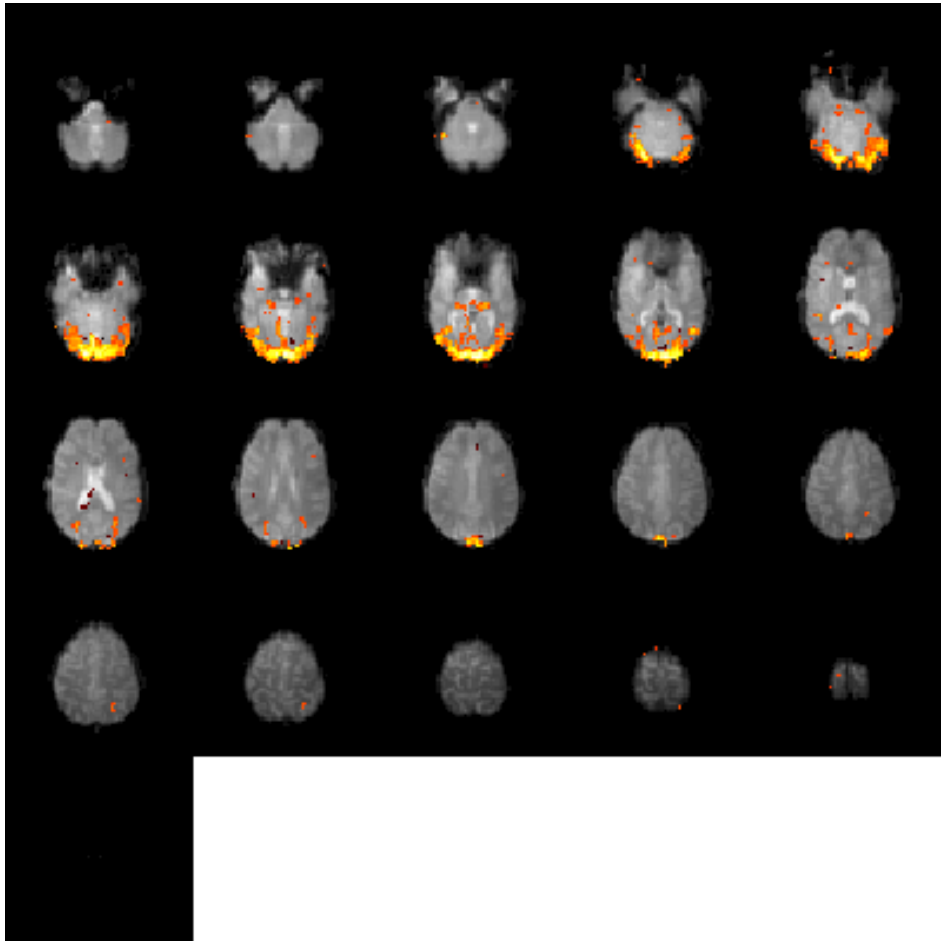

Figure 4: Axial slices of the functional MRI data with with the statistical image overlayed. The test statistics were thresholded at $|Z| \geq 4$.

3   Motion Correction and Co-registration

Basic motion correction within an acquisition, and co-registration between acquired series, is available using template matching (`en.wikipedia.org/wiki/Template_matching`). A reference volume must be pre-specified where a mask has been applied to remove all voxels that should not be included in the algorithm. Note, only three-dimensional translations are allowed and no interpolation is used (i.e., only whole-voxel translations) at this time.

4   T1 Relaxation and Gadolinium Concentration

Estimation of the tissue T1 relaxation rate is the first step in converting signal intensity, obtained in the dynamic acquisition of the DCE-MRI protocol, to contrast agent concentration. The subsequent steps provided here focus on pharmacokinetic modeling and assumes one has converted the dynamic acquisition to contrast agent concentration. Please see Collins and Padhani (2004) for a discussion on this point.

There are a miriad of techniques to quantify T1 using MRI. Currently curve-fitting methods for two popular acquisition schemes are available

- Inversion recovery (`www.e-mri.org/mri-sequences/inversion-recovery-stir-flair.html`)

- Multiple flip angles (Parker and Padhani, 2003)

Once the tissue T1 relaxation rate has been estimated, the dynamic acquisition is then converted to contrast agent concentration. Note, the B1 field is assumed to be constant (and accurate) when using multiple flip angles to estimate T1. At higher fields strengths (e.g., 3T) the B1 field should be estimated in order to correct the prescribed flip angles.

4.1   B1 Mapping Via the Saturated Double-Angle Method

For in vivo MRI at high field ($\geq$ 3Tesla) it is essential to consider the homogeneity of the active B1 field (B1+). The B1+ field is the transverse, circularly polarized component of B1 that is rotating in the same sense as the magnetization. When exciting or manipulating large collections of spins, nonuniformity in B1+ results in nonuniform treatment of spins. This leads to spatially varying image signal and image contrast and to difficulty in image interpretation and image-based quantification (Cunningham *et al.*, 2006).

The proposed method uses an adaptation of the double angle method (DAM). Such methods allow calculation of a flip-angle map, which is an indirect measure of the B1+ field. Two images are acquired: I_1 with prescribed tip α_1 and I_2 with prescribed tip $\alpha_2 = 2\alpha_1$. All other signal-affecting sequence parameters are kept constant. For each voxel, the ratio of magnitude images satisfies

$$\frac{I_2(r)}{I_1(r)} = \frac{\sin \alpha_2(r) f_2(T_1, \mathrm{TR})}{\sin \alpha_1(r) f_1(T_1, \mathrm{TR})}$$

where r represents spatial position and $alpha_1(r)$ and $\alpha_2(r)$ are tip angles that vary with the spatially varying B1+ field. If the effects of T_1 and T_2 relaxation can be neglected, then the

actual tip angles as a function of spatial position satisfy

$$\alpha(r) = \arccos\left(\left|\frac{I_2(r)}{2I_1(r)}\right|\right)$$

A long repetition time ($\mathrm{TR} \leq 5T_1$) is typically used with the double-angle methods so that there is no T_1 dependence in either I_1 or I_2 (i.e., $f_1(T_1, \mathrm{TR}) = f_2(T_1, \mathrm{TR}) = 1.0$. Instead, the proposed method includes a magnetization-reset sequence after each data acquisition with the goal of putting the spin population in the same state regardless of whether the or α_2 excitation was used for the preceding acquisition (i.e., $f_1(T_1, \mathrm{TR}) = f_2(T_1, \mathrm{TR}) \neq 1.0$.

4.2   Example

Using data acquired from a T1 phantom at two flip angles, $\alpha_1 = 60°$ and $\alpha_2 = 120°$, we compute the multiplicative factor relative to the low flip angle using the saturated double-angle method (Cunningham *et al.*, 2006).

```
> sdam60 <- read.img("SDAM_ep2d_60deg_26slc.nii.gz")
> dim(sdam60)
```

```
[1] 64 64 36 10
```

```
> sdam120 <- read.img("SDAM_ep2d_120deg_26slc.nii.gz")
> dim(sdam120)
```

```
[1] 64 64 36 10
```

```
> sdam.image <- rowMeans(dam(sdam60, sdam120, 60), dims = 3)
> mask <- rowSums(sdam60, dims = 3) > 500
```

Figure 5 is the estimated B1+ field (with isotropic Gaussian smoothing) for a T1 phantom containg a variety of T1 relaxation times. The center of the phantom exhibits a flip angle $> 60°$ while the flip angle rapidly becomes $< 60°$ when moving away from the center in either the x, y or z dimensions. Isotropic smoothing should be applied before using this field to modify flip angles associated with additional acquisitions (e.g., in the **AnalyzeFMRI** package).

Assuming the smoothed version of the B1+ field has been computed (`SDAM`), multiple flip-angle acquistions can be used to estimate the T1 relaxation rate from the subject (or phantom). The multiplicative factor, derived from the saturated double-angle method, is used to produce a spatially-varying flip-angle map and input into the appropriate function.

```
> TR <- 4.22/1000
> fanglesB1 <- fangles * array(SDAM[, , 1:26], c(X, Y, Z, nangles))
> R1 <- R1.fast(flip, mask[, , 1:26], fanglesB1, TR, verbose = TRUE)
```
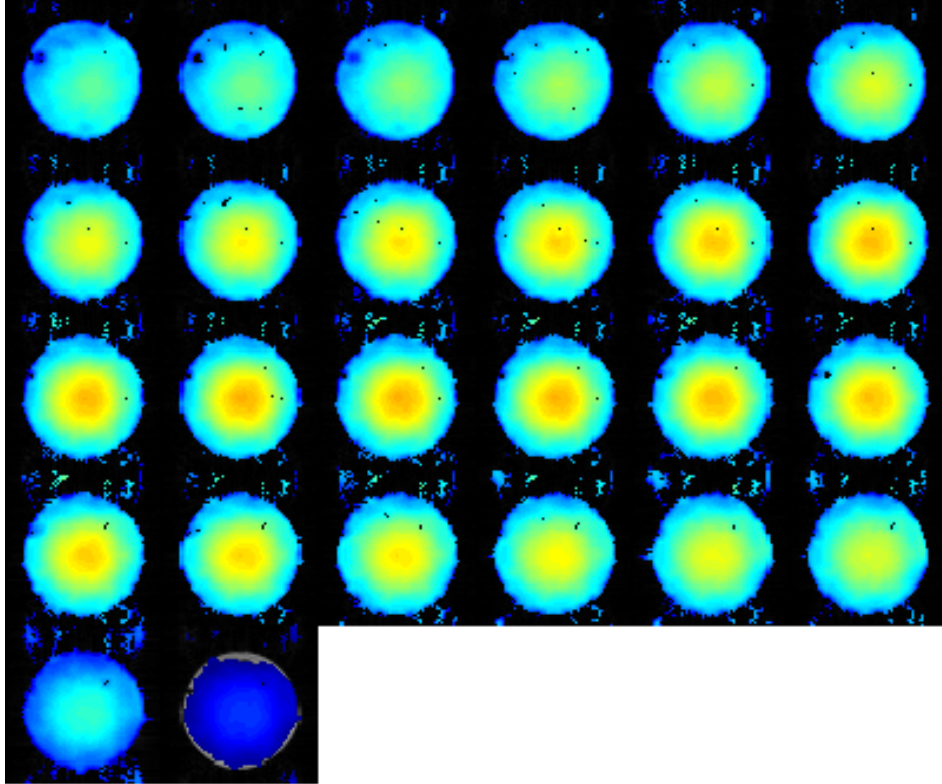
Figure 5: Estimated B1+ field (with isotropic Gaussian smoothing) using the saturated double-angle method. The colors correspond to a multiplicative factor relative to the true flip angle (60°).

```
    Deconstructing data...
    Calculating R10 and M0...

This product includes software developed by the University of Chicago, as
Operator of Argonne National Laboratory.

See the LICENSE file distributed with the minpack.lm source code or
http://www.netlib.org/minpack/disclaimer for the full license.

    Reconstructing results...
```

Figure 6 displays the quantitative T1 map for the phantom using information from the estimated B1+ field.
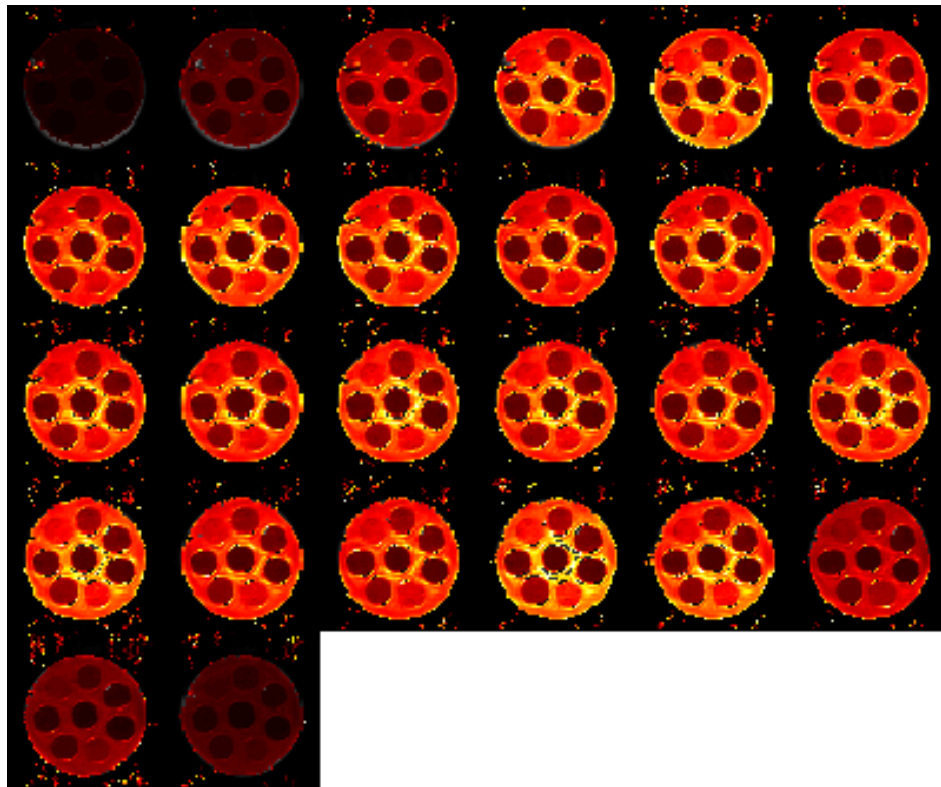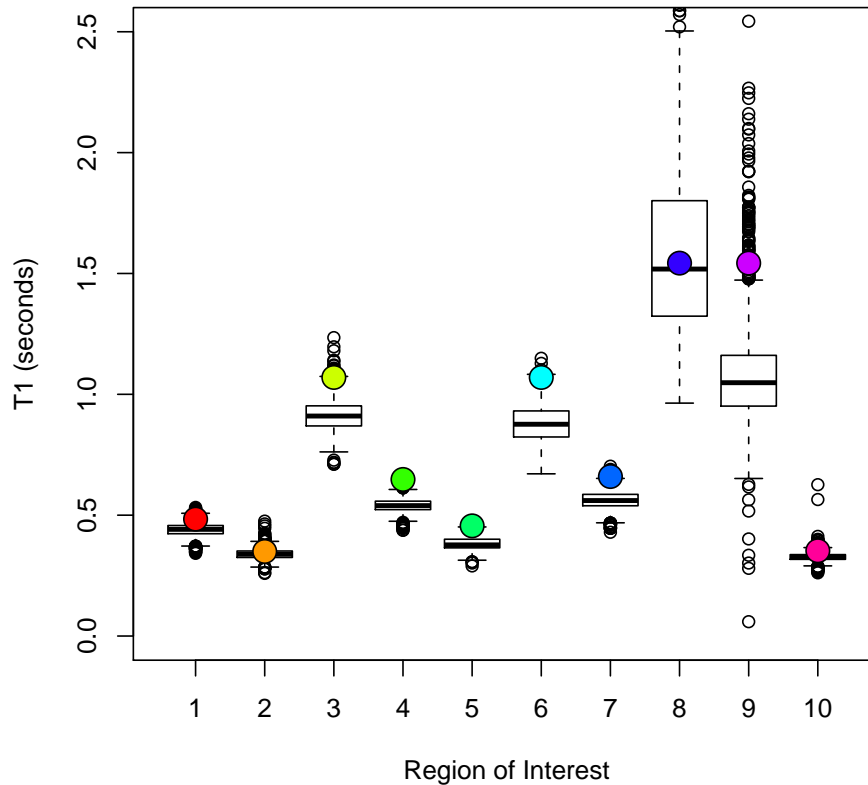

Figure 6: Estimated T1 relaxation rates for the phantom data acquisition. The colors range from 0-2.5 seconds.

By defining regions of interest (ROIs) in

```
> pmask <- read.img("t1_phantom_mask.nii.gz")
> dim(pmask)
```

```
[1] 64 64 26  1

> pmask[, , c(1:24, 26), 1] <- pmask[, , 25, 1]
```


we may compare the "true" T1 values for each ROI with those obtained from acquiring multiple flip angles with the application of B1 mapping. Figure 4.2 compares T1 estimates in the 10 ROIs, defined by `pmask`, with the true T1 values (large circles). The first seven ROIs correspond to the cylinders that run around the phantom, clockwise starting from approximatley one o'clock. The eighth and ninth ROIs are taken from the main compartment in the phantom; ROI eight is drawn in the middle of the phantom while ROI nine is drawn from the outside of the phantom. The final ROI is taken from the central cylinder embedded in the phantom.

4.3   Contrast Agent Concentration

The `CA.fast` function rearranges the assumed multidimensional (2D or 3D) structure of the multiple flip-angle data into a single matrix to take advantage of internal R functions instead of loops, and called `E10.lm`. Conversion of the dynamic signal intensities to contrast agent

concentration is performed via

$$[\text{Gd}] = \frac{1}{r_1} \left(\frac{1}{T_1} - \frac{1}{T_{10}} \right),$$

where r_1 is the spin-lattice relaxivity constant and T_{10} is the spin-lattice relaxation time in the absence of contrast media (Buckley and Parker, 2005). For computational reasons, we follow the method of Li *et al.* (2000).

4.4   Arterial Input Function

Whereas quantitative PET studies routinely perform arterial cannulation (`en.wikipedia.org/wiki/Cannula`) on the subject in order to characterize the arterial input function (AIF), it has been common to use literature-based AIFs in the DCE-MRI literature. Examples include

$$C_p(t) = D \left(a_1 e^{m_1 t} + a_2 e^{m_2 t} \right),$$

where $D = 0.1\,\text{mmol/kg}$, $a_1 = 3.99\,\text{kg/l}$, $a_2 = 4.78\,\text{kg/l}$, $m_1 = 0.144\,\text{min}^{-1}$ and $m_2 = 0.0111\,\text{min}^{-1}$ (Weinmann *et al.*, 1984; Tofts and Kermode, 1984); or $D = 1.0\,\text{mmol/kg}$, $a_1 = 2.4\,\text{kg/l}$, $a_2 = 0.62\,\text{kg/l}$, $m_1 = 3.0$ and $m_2 = 0.016$ (Fritz-Hansen *et al.*, 1996). There has been progress in measuring the AIF using the dynamic acquisition and fitting a parametric model to the observations. Recent models include Parker *et al.* (2006) and Orton *et al.* (2008). **dcemri** has incorporated two of the parametric models

$$
\begin{aligned}
C_p(t) &= A_B t e^{-\mu_B t} + A_G \left(e^{-\mu_G t} + e^{-\mu_B t} \right) \\
C_p(t) &= \begin{cases} a_B \left(1 - \cos(\mu_B t) \right) + a_B a_G f(t, \mu_G) & 0 \le t \le t_B \\ a_B a_G f(t, \mu_G) e^{-\mu_G(t - t_B)} & t > t_B \end{cases}
\end{aligned}
$$

(Orton *et al.*, 2008) into the kinetic parameter estimation step. While default values for each model are provided, there is also the ability to include user-specified parameters.

5   Kinetic Parameter Estimation

The standard Kety model (Kety, 1960), a single-compartment model, or the extended Kety model, the standard Kety model with an extra "vascular" term, form the collection of basic parametric models one can apply using **dcemri**. Regardless of which parametric model is chosen for the biological system, the contrast agent concentration curve at each voxel in the region of interest (ROI) is approximated using the convolution of an arterial input function (AIF) and the compartmental model; e.g.,

$$
\begin{aligned}
C_t(t) &= K^{\text{trans}} \left[C_p(t) \otimes e^{-k_{\text{ep}} t} \right], \\
C_t(t) &= v_{\text{p}} C_P(t) + K^{\text{trans}} \left[C_p(t) \otimes e^{-k_{\text{ep}} t} \right].
\end{aligned}
$$

Parameter estimation is achieved using one of two options in the current version of this software:

- Non-linear regression using non-linear least squares (Levenburg-Marquardt optimization)

- Bayesian estimation using Markov chain Monte Carlo (MCMC) (Schmid *et al.*, 2006)

Least-square estimates of the kinetic parameters K^{trans} and k_{ep} (also v_{p} for the extended Kety model) are provided in `dcemri.lm` while the posterior median is provided in `dcemri.bayes`. When using Bayesian estimation all samples from the joint posterior distribution are also provided, allowing one to interrogate the empirical probability density function (PDF) of the parameter estimates.

6   Statistical Inference

No specific support is provided for hypothesis testing in **dcemri**. We recommend one uses builtin facilities in R to perform ANOVA (analysis of variance) or mixed-effects models based on statistical summaries of the kinetic parameters over the ROI per subject per visit. An alternative to this traditional approach is to analyze an entire study using a Bayesian hierarchical model (Schmid *et al.*, 2009), available in the software project **PILFER** (`pilfer.sourceforge.net`) .

One may also question the rationale for hypothesis testing in only one kinetic parameter. Preliminary work has been performed in looking at the joint response to treatment of both K^{trans} and k_{ep} in DCE-MRI by O'Connor *et al.* (2010).

References

Buckley, D. L. and G. J. M. Parker (2005). Measuring contrast agent concentration in T$_1$-weighted dynamic contrast-enhanced MRI. In A. Jackson, D. L. Buckley, and G. J. M. Parker (Eds.), *Dynamic Contrast-Enhanced Magnetic Resonance Imaging in Oncology*, pp. 69–80. Berlin: Springer.

Collins, D. J. and A. R. Padhani (2004). Dynamic magnetic resonance imaging of tumor perfusion. *IEEE Engineering in Biology and Medicine Magazine*, 65–83.

Cunningham, C., J. Pauly, and K. Nayak (2006). Saturated double-angle method for rapid B1+ mapping. *Magnetic Resonance in Medicine 55*, 1326–1333.

Fritz-Hansen, T., E. Rostrup, H. B. W. Larsson, L. Søndergaard, P. Ring, and O. Henriksen (1996). Measurement of the arterial concentration of Gd-DTPA using MRI: A step toward quantitative perfusion imaging. *Magnetic Resonance in Medicine 36*, 225–231.

Kety, S. (1960). Blood–tissue exchange methods. Theory of blood-tissue exchange and its application to measurement of blood flow. *Methods in Medical Research 8*, 223–227.

Li, K.-L., X. P. Zhu, J. Waterton, and A. Jackson (2000). Improved 3D quantitative mapping of blood volume and endothelial permeability in brain tumors. *Journal of Magnetic Resonance Imaging 12*, 347–357.

O'Connor, E., N. Fieller, A. Holmes, J. C. Waterton, and E. Ainscow (2010). Functional principal component analyses of biomedical images as outcome measures. *Journal of the Royal Statistical Society C (Applied Statistics)*. in press.

Orton, M. R., J. A. d'Arcy, S. Walker-Samuel, D. J. Hawkes, D. Atkinson, D. J. Collins, and M. O. Leach (2008). Computationally efficient vascular input function models for quantitative kinetic modelling using DCE-MRI. *Physics in Medicine and Biology 53*, 1225–1239.

Parker, G. J. M. and A. R. Padhani (2003). T_1-w DCE-MRI: T_1-weighted dynamic contrast-enhanced MRI. In P. Tofts (Ed.), *Quantitative MRI of the Brain: Measuring Changes Caused by Disease*, Chapter 10, pp. 341–364. Chichester, UK: Wiley.

Parker, G. J. M., C. Roberts, A. Macdonald, G. A. Buonaccorsi, S. Cheung, D. L. Buckley, A. Jackson, Y. Watson, K. Davies, and G. C. Jayson (2006). Experimentally-derived functional form for a population-averaged high-temporal-resolution arterial input function for dynamic contrast-enhanced MRI. *Magnetic Resonance in Medicine 56*, 993–1000.

Schmid, V., B. Whitcher, A. R. Padhani, N. J. Taylor, and G.-Z. Yang (2006). Bayesian methods for pharmacokinetic models in dynamic contrast-enhanced magnetic resonance imaging. *IEEE Transactions on Medical Imaging 25*(12), 1627–1636.

Schmid, V. J., B. Whitcher, A. R. Padhani, N. J. Taylor, and G.-Z. Yang (2009). A Bayesian hierarchical model for the analysis of a longitudinal dynamic contrast-enhanced MRI oncology study. *Magnetic Resonance in Medicine 61*(1), 163–174.

Tofts, P. S. and A. G. Kermode (1984). Measurement of the blood-brain barrier permeability and leakage space using dynamic MR imaging. 1. Fundamental concepts. *Magnetic Resonance in Medicine 17*(2), 357–367.

Weinmann, H. J., M. Laniado, and W. Mutzel (1984). Pharmacokinetics of Gd-DTPA/dimeglumine after intraveneous injection into healthy volunteers. *Physiological Chemistry and Physics and Medical NMR 16*, 167–172.